Zintl Phases

DOI: 10.1002/anie.201301540

$LiBSi_2$: A Tetrahedral Semiconductor Framework from Boron and Silicon Atoms Bearing Lithium Atoms in the Channels**

Michael Zeilinger, Leo van Wüllen, Daryn Benson, Verina F. Kranak, Sumit Konar, Thomas F. Fässler, and Ulrich Häussermann**

Dedicated to Prof. Dr. Dr. h. c. mult. Wolfgang A. Herrmann on the occasion of his 65th birthday

The crystalline open frameworks of zeolites and clathrates are based on three-periodic, four-connected nets with tetrahedral nodes and have long attracted attention for their unique physical properties and great significance to fundamental crystal chemistry.[1] Such open tetrahedral frameworks (OTFs) enclose interstitial volumes in the form of large and separated cages (clathratic frameworks) or channels (zeolitic frameworks). While they most commonly occur with oxide materials, using oxygen to bridge the tetrahedral nodes, intermetallic Zintl phases may realize OTFs where the edges of nets correspond to covalent two-center, two-electron bonds (direct links).[2] Tetrahedral nodes in Zintl-phase OTFs are typically represented by the tetravalent Group 14 element (Tt) atoms Si, Ge, and Sn or mixtures of Tt atoms and trivalent Group 13 element (Tr) atoms (sp^3 hybridized atoms). For the latter systems, the apparent electron deficiency is balanced by electrons of the less electronegative metals situated in cavities in the OTF (guest species), which becomes nominally charged, that is, $(4c\text{-}Tt)_n = (A^+)_m(4c\text{-}Tt)_{n-m}(4c\text{-}Tr^-)_m$ (4c = four-connected, A = alkaline-earth metal) and thus shows a strong analogy to the charge distribution in aluminosilicates.

Among Zintl-phase OTFs the clathrate-I and -II type of structures with the nets **mtn** and **mep**, respectively,[3] are most prominent (Scheme 1). They occur for numerous compositions and have received considerable attention for their thermoelectric and superconducting properties.[4] Guest species in cages (i.e. Na–Cs, Sr, Ba, Eu atoms) play an important role in determining and tuning electric and thermal transport properties.[2a] Other OTFs include zeolitic frameworks such as the chiral net **unj** which is the basis of the structures of $NaInSn_2$, $NaGaSn_2$, and $NaGaSn_5$ as well as *hP*-Na_2ZnSn_5 and *tI*-Na_2ZnSn_5,[5] and **CAS** which describes the topology of the frameworks of $Eu_4Ga_6Si_{16}$ or ASi_6 (A = Ca, Sr, Ba).[6]

Notably, compared with silicates the topological variety of Zintl-phase OTFs is very limited[3a,7] and especially attempts to achieve Zintl-phase OTFs with Li as the guest species have long been unsuccessful,[8] although interesting properties for such materials were predicted.[9] For clathratic frameworks it

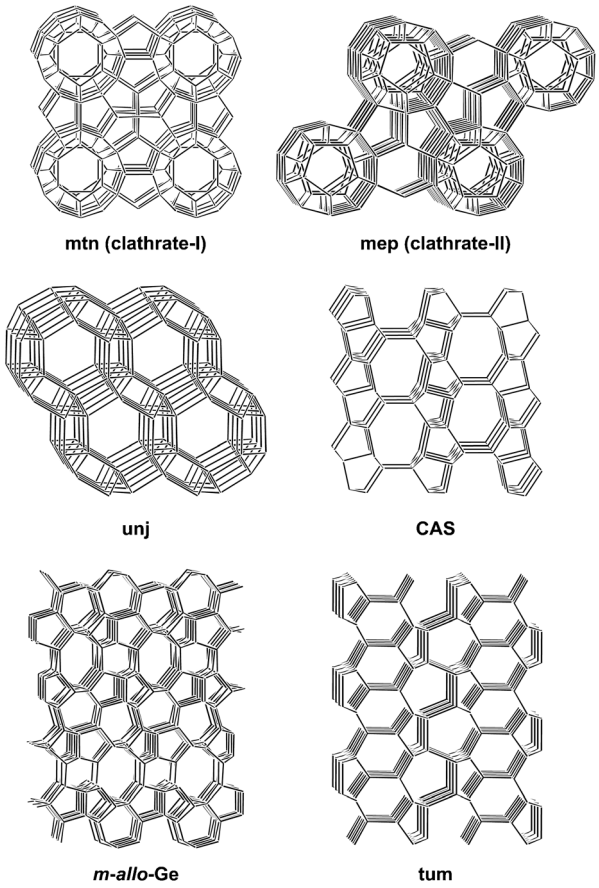

Scheme 1. Open tetrahedral frameworks realized by Zintl phases and Group 14 elements.[3]

[*] M. Zeilinger, Prof. Dr. T. F. Fässler
Department of Chemistry, Technische Universität München, Lichtenbergstrasse 4, 85747 Garching/München (Germany)
E-mail: thomas.faessler@lrz.tum.de
Prof. Dr. L. van Wüllen
Department of Physics, University of Augsburg, Universitätsstrasse 1, 86159 Augsburg (Germany)
D. Benson
Department of Physics, Arizona State University, Tempe, Arizona 85287-1504 (USA)
V. F. Kranak, S. Konar, Prof. Dr. U. Häussermann
Department of Materials and Environmental Chemistry, Stockholm University, SE-10691 Stockholm (Sweden)
E-mail: Ulrich.Haussermann@mmk.su.se

[**] This work was supported by Fonds der Chemischen Industrie, TUM Graduate School, Deutsche Forschungsgemeinschaft FA 198/11-1, the Swedish Research Council under contract number 2010-4827, and the National Science Foundation through grant DMR-1007557.

Supporting information for this article (including further details on the synthesis procedure, the analysis of products, and the computational procedure) is available on the WWW under http://dx.doi.org/10.1002/anie.201301540.

is believed that cages would be too large for Li atoms.[8] The encapsulation of Li atoms (in a stable compound) will probably require the OTF to consist of a large fraction of light elements from the second row, that is, B and C atoms. Thus far, the only known OTF involving a second row element is found in $K_7B_7Si_{39}$,[10] where a comparatively small fraction of the Si atoms in a clathrate-I structure are replaced by B atoms. Although this produced the smallest lattice parameter among Zintl phases with the clathrate-I structure cage, the size remained far too large for Li atoms.

Herein, we report on $LiBSi_2$ displaying a zeolitic framework with a new topology based on a unique strictly ordered distribution of B and Si atoms. This B-Si OTF has mutually orthogonal channels that host Li atoms.

$LiBSi_2$ was obtained as a dark gray, microcrystalline, powder from reaction mixtures LiB:Si = 1:1 that had been pressurized to 10 GPa and heated at 900 °C. $LiBSi_2$ is air and moisture stable, and also inert to strong acids. Its thermal stability exceeds 800 °C. The structure of $LiBSi_2$ depicted in Figure 1 was solved from powder X-ray diffraction data using a parallel tempering algorithm and subsequently finalized by Rietveld refinement.[11]

$LiBSi_2$ crystallizes with the tetragonal space group $P4_2/nmc$ and contains eight formula units in the unit cell

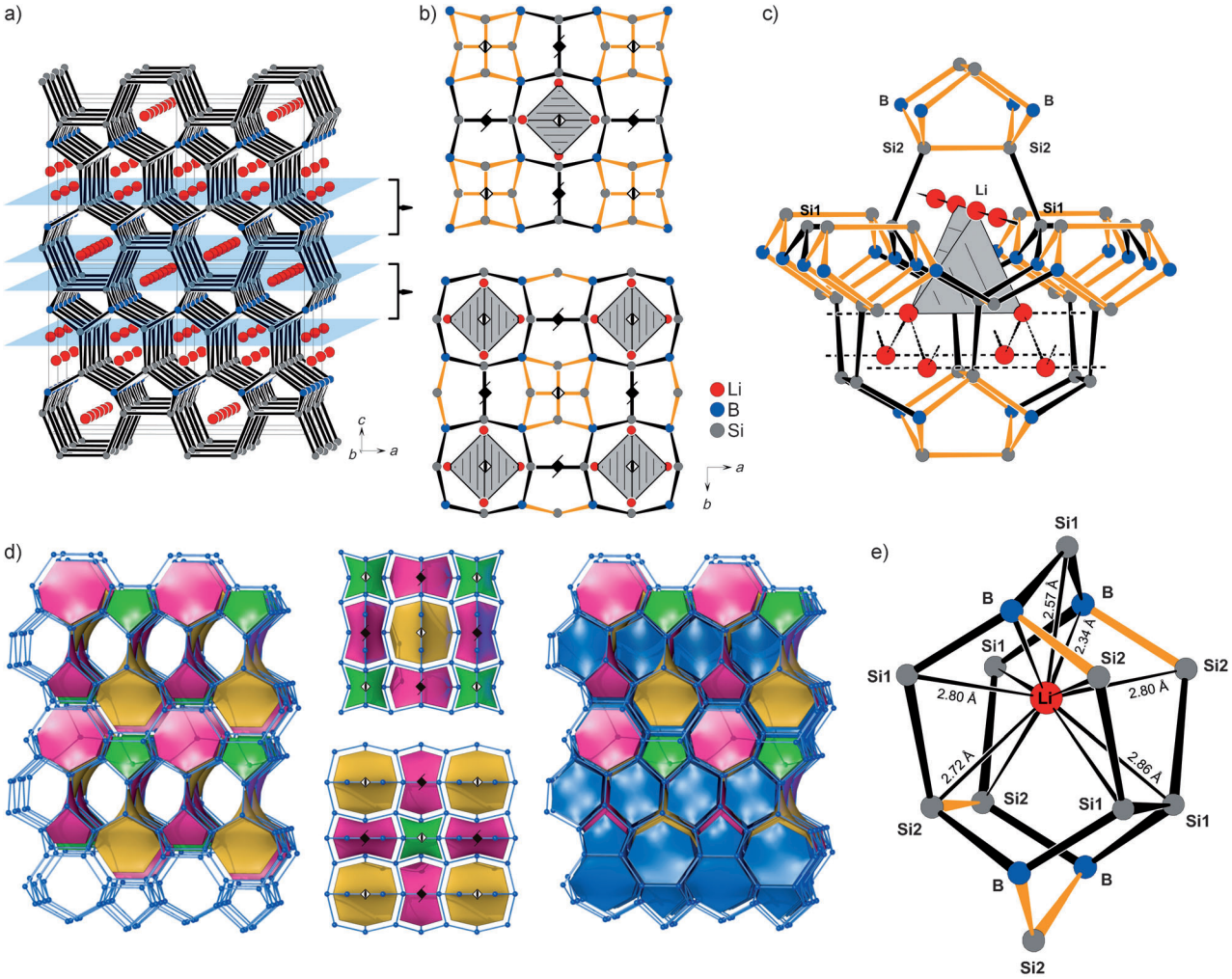

Figure 1. a) Crystal structure of tetragonal $LiBSi_2$ (2×2×2 supercell) viewed approximately along the [100] direction. Atoms are displayed as ellipsoids at a 90% probability (Li red, B blue, Si dark gray). Boundaries of two slab-like building units are marked by light blue planes. b) Two consecutive slab building units projected along the [001] direction. Bonds of the realgar-like $[B_4Si2_4]$ structural unit are drawn in yellow. Elongated tetrahedra produced by the arrangement of Li atoms are highlighted. The position of 4_2 and $\bar{4}$ axes are indicated by their symbol. c) Section of the $LiBSi_2$ structure showing the consequence of connecting slab building units: six- and seven-membered rings are introduced defining orthogonal channels that host the Li atoms. Within seven-ring channels Li atoms are arranged as linear chains, within six-ring channels as zigzag chains. Connecting lines between Li atoms do not indicate interactions, they are only meant to emphasize structural features. d) Natural tiling for the net **tum** formed by B and Si atoms in $LiBSi_2$. There are four different kinds of tiles, three four-faced tiles and one six-faced. (A tile is characterized by a face symbol $[M^m.N^n...]$ indicating that there are m faces that are M-rings, n faces that are N-rings, and so on). Left: Arrangement of 4-faced tiles $[5^4]$ (green), $[7^4]$ (yellow), and $[5^2.7^2]$ (pink) not sharing faces. Middle: Arrangement of four-faced tiles within slab building blocks (Figure 1b). Right: Complete natural tiling of **tum** including also the six-faced "Li tiles" $[5^2.6^2.7^2]$ (blue). Li tiles share common six-ring faces which emphasizes the six-ring channel system (hosting Li zigzag chains) in zeolitic $LiBSi_2$ (seen at the bottom of the figure). e) Coordination environment around Li atoms within a $[5^2.6^2.7^2]$ tile.

(Figure 1a). The B-Si ordered OTF is built from three distinct crystallographic positions—one B site (8*f*) and two Si sites (Si1 and Si2, both on 8*g*)—and thus corresponds to a trinodal net. Li atoms are situated on an *8g* site and occupy channels in the B-Si OTF.

The tetrahedral B-Si framework can be divided into $[B_4Si2_4]$ realgar-like units and Si1-Si1 dumbbells which occur in a 1:2 ratio and are arranged in two-dimensional slabs (Figure 1b). The realgar-like unit represents a cage, which is enclosed by four five-membered rings. Its linkage with the $Si1_2$ dumbbell units creates additional five-membered rings. The slab also contains eight-membered rings, which, however, become part of seven-membered rings upon connecting slabs and thus do not represent strong rings in the three-periodic framework.[12] Finally, a slab hosts mutually perpendicular linear chains of Li atoms at two different heights (corresponding to the thickness of a slab; Figure 1a) running along the *a* and *b* directions. Distances in a linear chain are alternating short (3.36 Å) and long (3.47 Å), and the arrangement of short distances corresponds to elongated Li_4 tetrahedra surrounded by eight-membered rings.

In the three-periodic net, slabs are stacked along the *c* direction, related by the *n* glide perpendicular to *c* (Figure 1b). As a consequence, realgar and Li_4 tetrahedral units are situated alternating on top of each other and $(Si1)_2$ dumbbells are stacked mutually rotated by 90°.[13] The connection of slabs introduces six- and seven-membered rings, which define the channels hosting the Li atoms (Figure 1c, compared to Figure 1a). In channels embraced by seven-membered rings, Li atoms are arranged as the linear chains mentioned above; in channels embraced by six-membered rings, Li atoms form zigzag chains where they are equidistantly separated at 3.66 Å (Figure 1c). This distance corresponds to the separation of Li_4 tetrahedra, or alternatively the distance between parallel linear chains at different heights. Both kinds of channels run along the *a* and *b* directions and are mutually converted by a 90° rotation around the *c* axis.

The outcome of the ordering of B and Si atoms is that B atoms are exclusively bonded to Si atoms with $d_{Si\text{-}B} = 2.05$ and 2.08 Å whereas Si atoms utilize two homoatomic bonds with distances $d_{Si\text{-}Si} = 2.44$, 2.47, and 2.51 Å. Different B–Si and Si–Si bond lengths induce distorted tetrahedral coordination environments ($\sphericalangle$(Si–B–Si) = 91.07°–124.52°; $\sphericalangle$(B–Si–B) = 106.41°, 117.30°; $\sphericalangle$(Si–Si–B) = 100.94°–116.96°; $\sphericalangle$(Si–Si–Si) = 112.33°).

The OTF formed by B and Si atoms in $LiBSi_2$ consists exclusively of five-, six-, and seven-membered rings and represents a not yet described topology for a three-periodic, four-connected net. It has been assigned the symbol **tum** in the TTD topological database.[14] We note that **tum** is also the net of the orthorhombic framework of the recently discovered intermetallic compounds $Na_5M_{2+x}Sn_{10-x}$ ($x \approx 0.5$, M = Zn, Hg) where it is formed by the M and Sn atoms.[15]

The natural tiling associated with **tum** is shown in Figure 1d. A tiling is the filling of space by generalized polyhedra (tiles) that share faces.[16] A tile represents the interior of a cage with typically curved faces that are rings of the net. Thus a tiling carries a net formed by the vertices and edges of tiles. According to a set of rules, natural tilings are unique and provide an unambiguous way to partition space by the net. This in turn enables convenient identification and analysis of the size and location of cavities and channels. For **tum** there are four kinds of tiles: one corresponds to the $[B_4Si2_4]$ realgar-like cage centered at the Wyckoff site 2a and has the face symbol $[5^4]$, indicating that there are four faces that are five-membered rings. Another tile with face symbol $[7^4]$ is located at the center of the Li_4 tetrahedron (position 2b) and a third tile with the face symbol $[5^2.7^2]$ is centered at site 4d, in between two $Si1_2$ dumbbells stacked along the *c* direction. The fourth tile is enclosed by six faces (face symbol $[5^2.6^2.7^2]$) and is centered at a position approximately corresponding to the location of the Li atoms (Figure 1e).

This partitioning appears chemically meaningful; the three four-faced tiles do not share common faces but are tetrahedrally surrounded by Li tiles, which in turn are octahedrally connected to two $[5^2.7^2]$ tiles (through a seven- and a five-membered ring face, respectively), one realgar $[5^4]$ tile, one $[7^4]$ tile, and two other Li tiles (sharing six-sided faces). The face sharing of Li tiles defines the relevant channels (Figure 1f), which, interestingly, are those that are embraced by six-membered rings and host zigzag chains of Li atoms rather than the ones embraced by seven-membered rings that host linear chains. Li atoms in $LiBSi_2$ attain a clearly defined coordination by two B and nine Si atoms (Figure 1e). Distances range from 2.34 Å (Li-B) to 2.86 Å (Li-Si1) and are well separated from the next nearest neighbor distances starting off at 3.34 Å (Li-B). However, the tile (cage) associated with Li is larger (14 vertices) and Li is positioned quite off-centered in its tile.

The structure was further confirmed by the Raman spectrum of $LiBSi_2$ (Figure 2). The rather complex structure gives rise to 31 Raman-active modes,[17] of which about 20 are observed. Excitation with a green laser ($\lambda = 532$ nm) yields better resolved high-frequency modes, whereas red-laser excitation ($\lambda = 785$ nm) results in better resolved low-frequency modes. The assignment of bands was assisted by first-principles zone center phonon calculations. The modes with lowest and highest wave number were calculated at 168 and 683 cm^{-1}, respectively, which is in good agreement with the span of wave numbers of the observed spectrum. The bands in the wave number region 600–700 cm^{-1} correspond to B-Si vibrations (modes 14–19; Figure 2) and are detached from the bulk of modes between 150 and 470 cm^{-1}. The latter range of wave numbers is typical for Si-Si stretching and bending vibrations in silicide clathrates,[18] however, for $LiBSi_2$ we find that bands from Si-Si and Li-Si vibrations appear at similar wave numbers. In fact, mode 13 at around 467 cm^{-1} corresponds to a Li-Si vibration, whereas the first Si-Si stretching mode (12) is at around 430 cm^{-1}. This indicates a strong interaction between Li and the host OTF. Also, the optical mode with the lowest wave number involves displacement contributions from all atoms and is not, as perhaps expected, dominated by Li atoms.

The electronic structure of $LiBSi_2$ has been calculated and the density of states (DOS) is shown in Figure 3. $LiBSi_2$ is a semiconductor with a band gap of 1.1 eV. Because DFT-calculated band gaps are known to be underestimated, the

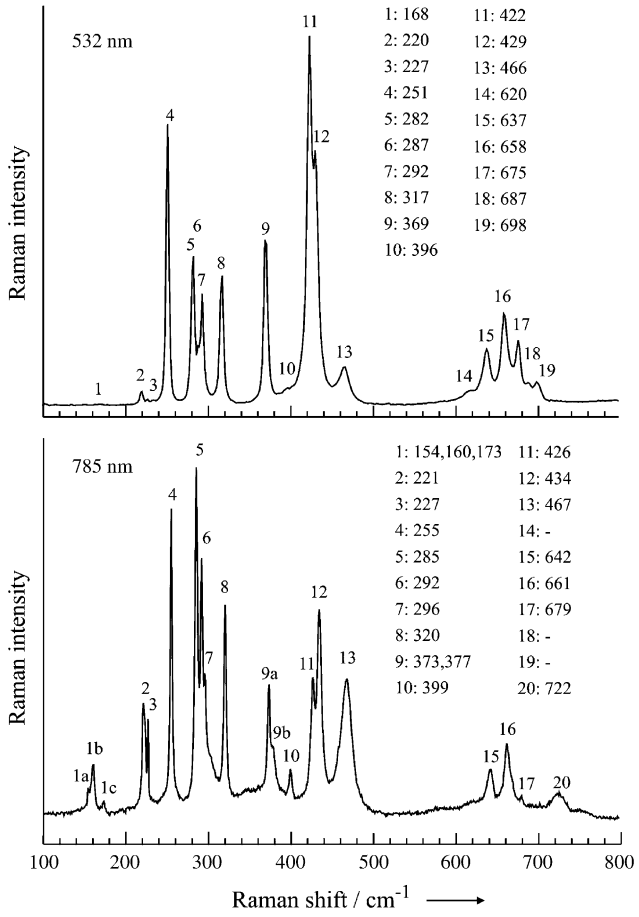

Figure 2. Raman spectrum of $LiBSi_2$ recorded with excitation wavelengths 532 and 785 nm. Values listed are wavenumbers (cm^{-1}) of the labeled bands (1–20). The origin of band 20 in the lower spectrum is not known.

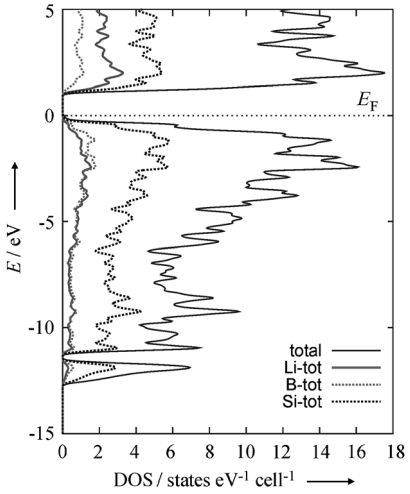

Figure 3. Electronic density of states for $LiBSi_2$ and the site projected contributions from Li, B, and Si atoms. The Fermi level (E_F) is set at 0 eV at the top of the valence band (dotted line).

experimental band gap may approach 2 eV. The occurrence of a band gap is in agreement with an electron precise B-Si OTF where Li acts as an electron donor, as expected for a Zintl phase. However, the site-projected DOS reveals that the Li and B states contribute almost equally and homogenously to the valence band throughout its range of dispersion. Such an intimate admixture of states from the less electronegative—electron-donating—component to the occupied valence band is not typical of a Zintl phase and is also indicative of strong Li-OTF interactions. Preliminary ^{7}Li- and ^{11}B-MAS-NMR investigations (chemical shift of ^{7}Li: −0.35 ppm) reveal the diamagnetic character. Further details on the NMR-spectroscopic investigations are given in the Supporting Information.

Apart from its new topology, the B-Si net in $LiBSi_2$ is also chemically unique: it represents the first example where B and Si atoms form an ordered common framework structure with boron exclusively engaged in heteronuclear B-Si contacts. Typically frameworks of borosilicides are characterized by either segregated B and Si structural entities or separated B_{12} icosahedra and Si_4 rhomboid rings as in β-SiB_3[19] or the occurrence of B/Si disorder as manifested in mixed occupied positions as, for example, in α-SiB_3, $Na_8B_{74.5}Si_{17.5}$,[20] and the earlier mentioned $K_7B_7Si_{39}$.[10] Since the **tum** net exclusively consists of four-connected nodes it additionally enlarges the number of models for novel tetrel allotropes, such as the recently predicted Si allotrope[21] or the experimentally established *m-allo*-Ge.[22]

In conclusion, we have shown that high-pressure reactions between LiB and Si afford $LiBSi_2$ with a novel intermetallic B-Si OTF dubbed **tum**. Unique to this compound is the encapsulation of small-sized Li as the guest species and the topology of the OTF, based on a strictly ordered distribution of B and Si atoms. Owing to the low density and its open framework structure, doped $LiBSi_2$ may be the basis for useful electrode materials.[9c] Also, **tum** may be an interesting model for a low-density allotrope of Group 14 elements. The search for such allotropes has recently become a very active field of research.[7,21] $LiBSi_2$ is predicted to be a semiconductor with a band gap exceeding 1 eV. Vibrational properties and the calculated electronic structure indicate that the Li guest species interacts strongly with the OTF host. The physical properties, the detailed formation conditions of $LiBSi_2$, as well as an analysis of the NMR-spectroscopic investigations will be presented in a forthcoming paper.

Experimental Section

In a typical synthesis a mixture of LiB and Si (80–100 mg, molar ratio 1:1) were sealed in a salt capsule. The capsules were compressed in a multi-anvil device[23] to a pressure of 10 GPa and subsequently heated to 900 °C at a rate of 5 °C min^{-1}. After equilibrating samples at their target temperature for one hour, the temperature was quenched and the pressure released at a rate of approximately 0.5 GPa per hour. The preparation of salt capsules and their recovery after high-pressure, high-temperature treatment was performed in an Ar-filled glove box. Thereafter, the product was treated with half concentrated HCl and washed several times with water and ethanol followed by drying in air. A synthesis run typically yielded 40–50 mg product. Products were analyzed by powder X-ray diffraction (PXRD), Raman, and ^{7}Li- and ^{11}B-MAS NMR spectroscopy.

Samples were ground, loaded into 0.3 mm capillaries, and measured on a STOE STADI P diffractometer (Ge-(111) monochromator for CuK_α radition, $\lambda = 1.54056$ Å) equipped with a linear position-sensitive detector (PSD). Tetragonal unit cell: $a =$ 6.83225(3) Å, $c = 8.83924(6)$ Å and space group $P4_2/nmc$. Further

details on the crystal structure may be obtained from the Fachinformationszentrum Karlsruhe, 76344 Eggenstein-Leopoldshafen, Germany (fax: (+49) 7247-808-666; e-mail: crysdata@fiz-karlsruhe.de), by quoting the depository number CSD-425643 ($LiBSi_2$).

Raman spectra were recorded on powder samples placed on a glass slide using a LabRAM HR 800 spectrometer with a back-thinned CCD detector and lasers at 532 and 785 nm as excitation sources. ^{7}Li- and ^{11}B-MAS (magic angle spinning) NMR spectra (Supporting Information, Figures S3,S4) were collected on a Varian VNMRs 500 spectrometer, operating at 160.37 MHz and 194.24 MHz for ^{11}B and ^{7}Li, respectively. MAS was performed at spinning speeds of 15–40 kHz with a Varian 1.6 mm triple resonance T^3-MAS probe. Theoretical calculations were performed in the framework of the frozen core all-electron projected augmented wave (PAW) method, as implemented in the program VASP.[24]

Received: February 22, 2013
Published online: April 22, 2013

Keywords: open tetrahedral frameworks · silicon · zeolites · Zintl phases

[1] a) J. V. Smith, *Chem. Rev.* **1988**, *88*, 149; b) M. O'Keeffe, B. G. Hyde, *Crystal Structures 1: Patterns and Symmetry*, Monograph, Mineralogical Assoc. of America, Washington DC, **1996**; c) O. Delgado Friedrichs, A. W. M. Dress, D. H. Huson, J. Klinowski, A. L. Mackay, *Nature* **1999**, *400*, 644.

[2] a) "Zintl Clathrates": A. V. Shevelkov, K. Kovnir in *Zintl Phases: Principles and Recent Developments*, *Vol. 139* (Eds.: D. M. P. Mingos, T. F. Fässler), Springer, Heidelberg **2011**, p. 97; b) "Structural Relationships Between Intermetallic Clathrates, Porous Tectosilicates and Clathrate Hydrates": D. Santamaria-Perez, F. Libeau in *Inorganic 3D Structures: The Extended Zintl-Klemm Concept*, *Vol. 138* (Eds.: D. M. P. Mingos, A. Vegas), Springer, Heidelberg **2011**, p. 1.

[3] Symbols for nets follow either the zeolite code according to ref. [3a] or the RCSR identifiers according to ref. [3b]; a) C. Baerlocher, W. M. Meier, D. H. Olson, *Atlas of Zeolite Framework Types*, 6th rev. ed., Elsevier, Amsterdam, **2007**. Data available online at http://www.iza-structure.org/databases/; b) M. O'Keeffe, M. A. Peskov, S. J. Ramsden, O. M. Yaghi, *Acc. Chem. Res.* **2008**, *41*, 1782.

[4] a) M. Beekman, G. S. Nolas, *J. Mater. Chem.* **2008**, *18*, 842; b) G. S. Nolas, J. L. Cohn, G. A. Slack, S. B. Schujman, *Appl. Phys. Lett.* **1998**, *73*, 178; c) S. Yamanaka, *Dalton Trans.* **2010**, *39*, 1901.

[5] a) W. Blase, G. Cordier, R. Kniep, R. Schmidt, *Z. Naturforsch. B* **1989**, *44*, 505; b) J. T. Vaughey, J. D. Corbett, *J. Am. Chem. Soc.* **1996**, *118*, 12098; c) W. Blase, G. Cordier, *Z. Naturforsch. B* **1988**, *43*, 1017; d) S. Stegmeier, S.-J. Kim, A. Henze, T. F. Fässler, unplublished results.

[6] a) J. D. Bryan, G. D. Stucky, *Chem. Mater.* **2001**, *13*, 253; b) W. Carrillo-Cabrera, S. Paschen, Y. Grin, *J. Alloys Compd.* **2002**, *333*, 4; c) A. Wosylus, Y. Prots, U. Burkhardt, W. Schnelle, U. Schwarz, *Sci. Technol. Adv. Mater.* **2007**, *8*, 383; d) A. Wosylus, Y. Prots, U. Burkhardt, W. Schnelle, U. Schwarz, Y. Grin, *Z. Naturforsch. B* **2006**, *61*, 1485; e) S. Yamanaka, S. Maekawa, *Z. Naturforsch. B* **2006**, *61*, 1493.

[7] a) M. M. J. Treacy, I. Rivin, E. Balkovsky, K. H. Randall, M. D. Foster, *Microporous Mesoporous Mater.* **2004**, *74*, 121; b) A. J. Karttunen, T. F. Fässler, M. Linnolahti, T. A. Pakkanen, *Inorg. Chem.* **2011**, *50*, 1733.

[8] Li replaces small amounts of Ge in the clathrate-I host structure. See: Y. Liang, B. Bohme, A. Ormeci, H. Borrmann, O. Pecher, F. Haarmann, W. Schnelle, M. Baitinger, Y. Grin, *Chem. Eur. J.* **2012**, *18*, 9818.

[9] a) A. Ker, E. Todorov, R. Rousseau, K. Uehara, F. X. Lannuzel, J. S. Tse, *Chem. Eur. J.* **2002**, *8*, 2787; b) N. Rey, A. Munoz, P. Rodriguez-Hernandez, A. San Miguel, *J. Phys. Condens. Matter* **2008**, *20*, 215218; c) A recent report gives evidence that Li can be inserted electrochemically into Si clathrate-II and may have potential as a novel electrode material for lithium-ion batteries, see: T. Langer, S. Dupke, H. Trill, S. Passerini, H. Eckert, R. Pöttgen, M. Winter, *J. Electrochem. Soc.* **2012**, *159*, A1318.

[10] W. Jung, J. Lorincz, R. Ramlau, H. Borrmann, Y. Prots, F. Haarmann, W. Schnelle, U. Burkhardt, M. Baitinger, Y. Grin, *Angew. Chem.* **2007**, *119*, 6846; *Angew. Chem. Int. Ed.* **2007**, *46*, 6725.

[11] a) F.O.X., Free Objects for Crystallography V 1.9.7.0, http://objcryst.sourceforge.net, **2011**; b) R. Černý, V. Favre-Nicolin, *Powder Diffr.* **2005**, *20*, 359; c) V. Favre-Nicolin, R. Cerny, *J. Appl. Crystallogr.* **2002**, *35*, 734; d) TOPAS 4.0—Rietveld Software, Bruker AXS, Madison (Wisconsin, USA), **2009**.

[12] Strong rings are defined as rings that are not the sum of any number of smaller cycles, see: O. Delgado-Friedrichs, M. O'Keeffe, *J. Solid State Chem.* **2005**, *178*, 2480.

[13] Realgar and Li_4 tetrahedral units have $-4m2$ symmetry. Note that the 4_2 screw axis runs through the centers of gravity of the $(Si1)_2$ units.

[14] a) V. A. Blatov, D. M. Proserpio, *Acta Crystallogr. Sect. A* **2009**, *65*, 202; b) V. A. Blatov, *IUCr CompComm. Newsletter* **2006**, *7*, 4; c) TOPOS Topological Databases and Topolgical Types Observed, http://www.topos.ssu.samara.ru.

[15] S. Ponou, S. J. Kim, T. F. Fässler, *J. Am. Chem. Soc.* **2009**, *131*, 10246.

[16] a) V. A. Blatov, O. Delgado-Friedrichs, M. O'Keeffe, D. M. Proserpio, *Acta Crystallogr. Sect. A* **2007**, *63*, 418; b) O. Delgado-Friedrichs, M. O'Keeffe, O. M. Yaghi, *Phys. Chem. Chem. Phys.* **2007**, *9*, 1035; c) V. A. Blatov, M. O'Keeffe, D. M. Proserpio, *CrystEngComm* **2010**, *12*, 44.

[17] E. Kroumova, C. Capillas, S. Ivantchev, H. Wondratschek, *Phase Transitions* **2003**, *76*, 155.

[18] a) G. S. Nolas, C. A. Kendziora, J. Gryko, J. Dong, C. W. Myles, A. Poddar, O. F. Sankey, *J. Appl. Phys.* **2002**, *92*, 7225; b) D. Machon, P. Toulemonde, P. F. McMillan, M. Amboage, A. Munoz, P. Rodriguez-Hernandez, A. San Miguel, *Phys. Rev. B* **2009**, *79*, 184101.

[19] J. R. Salvador, D. Bilc, S. D. Mahanti, M. G. Kanatzidis, *Angew. Chem.* **2003**, *115*, 1973; *Angew. Chem. Int. Ed.* **2003**, *42*, 1929.

[20] a) B. Magnusson, C. Brosset, *Acta Chem. Scand.* **1962**, *16*, 449; b) H. F. Rizzo, L. R. Bidwell, *J. Am. Ceram. Soc.* **1960**, *43*, 550; c) H. Morito, B. Eck, R. Dronskowski, H. Yamane, *Dalton Trans.* **2010**, *39*, 10197.

[21] a) M. A. Zwijnenburg, K. E. Jelfs, S. T. Bromley, *Phys. Chem. Chem. Phys.* **2010**, *12*, 8505; b) C. J. Pickard, R. J. Needs, *Phys. Rev. B* **2010**, *81*, 014106.

[22] a) A. Grüttner, R. Nesper, H. G. von Schnering, *Angew. Chem.* **1982**, *94*, 933; *Angew. Chem. Int. Ed. Engl.* **1982**, *21*, 912; b) F. Kiefer, A. J. Karttunen, M. Döblinger, T. F. Fässler, *Chem. Mater.* **2011**, *23*, 4578.

[23] E. Stoyanov, U. Häussermann, K. Leinenweber, *High Pressure Res.* **2010**, *30*, 175.

[24] a) P. E. Blöchl, *Phys. Rev. B* **1994**, *50*, 17953; b) G. Kresse, D. Joubert, *Phys. Rev. B* **1999**, *59*, 1758; c) G. Kresse, J. Hafner, *Phys. Rev. B* **1993**, *48*, 13115; d) G. Kresse, J. Furthmüller, *Comput. Mater. Sci.* **1996**, *6*, 15.

Angewandte Chemie
Eine Zeitschrift der Gesellschaft Deutscher Chemiker

Supporting Information

69451 Weinheim, Germany

$LiBSi_2$: A Tetrahedral Semiconductor Framework from Boron and Silicon Atoms Bearing Lithium Atoms in the Channels**

Michael Zeilinger, Leo van Wüllen, Daryn Benson, Verina F. Kranak, Sumit Konar, Thomas F. Fässler, and Ulrich Häussermann**

anie_201301540_sm_miscellaneous_information.pdf

Supporting Information

Synthesis. Starting materials were rods of Li (99 %, Rockwood-Lithium), boron chunks (99.95 %, ChemPur) and silicon powder (99.999%, Sigma-Aldrich). All steps for synthesis and sample preparation were carried out in a glove box (MBraun, Ar-atmosphere, H_2O and O_2 levels < 0.1 ppm). Stainless steel ampoules were thoroughly cleaned, heated to 700 °C under dynamic vacuum ($p < 1 \cdot 10^{-3}$ mbar) for at least 1 h and transferred to the glove box. Heating and handling under inert conditions was done by using an all-glass Schlenk line supplied with Ar, which is dried over phosphorous pentoxide, molecular sieve and heated titanium sponge (T = 750 °C).

LiB: Lithium and boron were filled into a stainless steel ampoule with a molar ratio of 1:1 and a total mass of 0.5 g. The ampoule was sealed by arc-welding inside the glove box and then encapsulated in a silica jacket under vacuum. After annealing at 470 °C in a muffle oven for three days pure LiB is obtained (Figure S1). For further synthesis steps LiB was ground inside an agate mortar.

$LiBSi_2$: High pressure syntheses were performed in a 6-8 Walker-type multi-anvil high pressure device using an 18/12 assembly developed by Stoyanov et al..[1] Mixtures of powdered LiB and Si with a molar ratio of 1:1 and a total amount between 80 and 100 mg were compacted and placed inside a NaCl capsule (inner diameter: 4 mm, outer diameter: 8 mm, length: 8 mm; prepared from NaCl dried under vacuum at 250-300 °C). Subsequently, capsules were sealed and transferred outside the glove box. To prepare the high pressure cell assembly NaCl sample capsules were positioned in a graphite furnace which in turn was placed together with a Zircon thermal insulating sleeve (0.57 mm wall thickness, 7.77 mm OD, 10.80 mm length) in a magnesia octahedron with 18 mm edge length. Samples were pressurized at a rate of about 0.5 GPa/h with 25 mm tungsten carbide cubes truncated to 12 mm edge length. After reaching the target pressure of 10 GPa the samples were heated. Deviations from the target pressure are estimated as +/– 0.3 GPa. The temperature was measured close to the sample using a thermocouple type C (W5%Re – W26%Re wire) in an Al_2O_3 sleeve. The samples were heated to 900 °C within 3 h. After applying a dwelling time of 1 h samples were quenched by turning off the power to the furnace (quench rate ~50 °C/min and at approximately constant pressure). Afterwards, the pressure was released at a rate of approximately 0.5 GPa/h and the samples were recovered in the glove box. Thereafter, the product was treated with diluted HCl and washed several times with water and ethanol followed by drying in air. The product was obtained as a fine, grey colored, powder. According to powder X-Ray diffraction it corresponds to crystalline $LiBSi_2$ and a minor amount of an unidentified crystalline impurity (Figure 2, reflections at 2θ ~21° and ~28°). Solid state NMR investigations (see below) revealed the presence of an amorphous byproduct next to crystalline $LiBSi_2$, which most likely is associated with the excess of LiB employed in the high pressure synthesis.

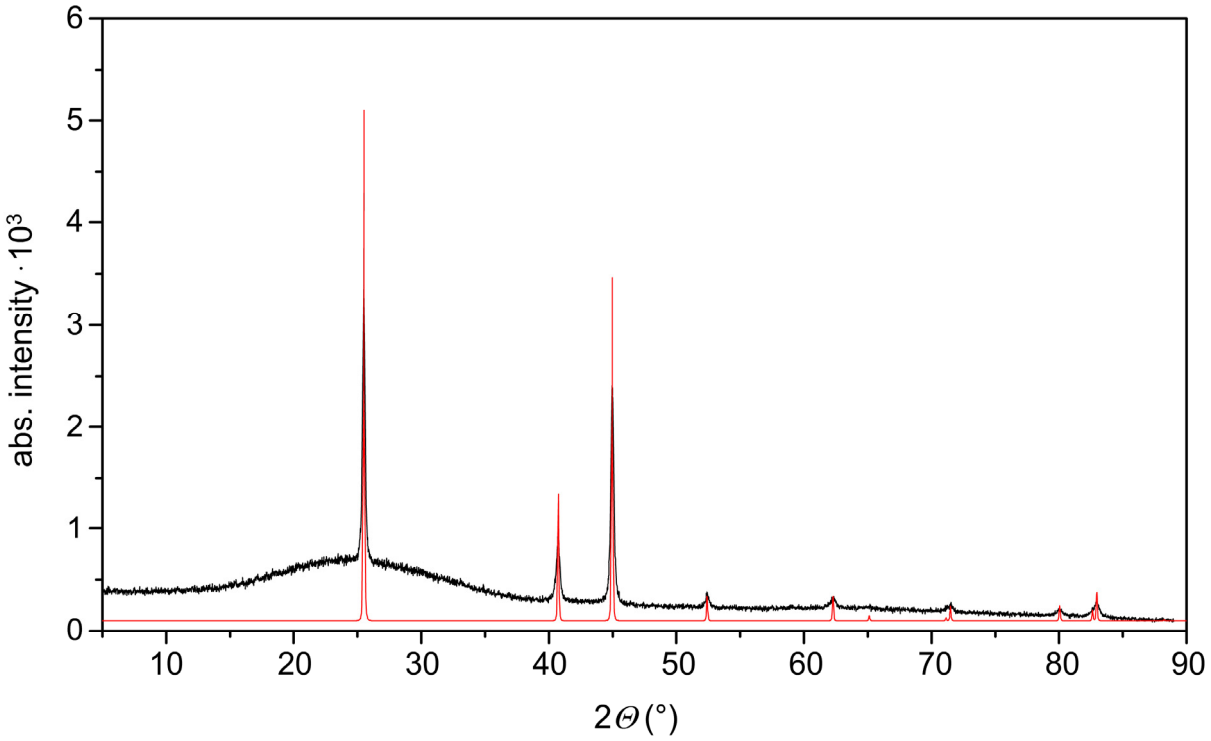

Figure S1. Experimental X-ray powder diffraction pattern of LiB (black) referenced with its theoretical powder pattern (red).

Powder X-ray diffraction. X-ray powder diffraction patterns were recorded on a STOE STADI P diffractometer (Ge-(111) monochromator for CuK_α radiation, $\lambda = 1.54056$ Å) equipped with a linear PSD. Samples were ground in an agate mortar, sealed in 0.3 mm glass capillaries and measured within a 2θ range of 5-90° using two measurement runs, each with a PSD step width of 0.05° and an exposure time of 40 sec per step.

Structure determination. The structure of $LiBSi_2$ was determined *ab initio* from X-ray powder diffraction data by using the parallel tempering algorithm implemented in the software FOX.[2] The X-ray diffraction pattern could be indexed with a tetragonal cell $a = 6.83225(3)$ Å, $c = 8.83924(6)$ Å and the space group $P4_2/nmc$ was assigned after Le Bail profile fitting. As the main idea of the FOX program is to approach structure solutions by starting with "structural building blocks" several structure motifs having B-B bonds could be excluded because Raman spectroscopy clearly showed the absence of those. Consequently, the idea of a tetrahedral B-Si network arose and resulted in a successful structure solution with acceptable reliability factors ($R_{wp} = 0.067$, GOF = 1.24). The final structure is provided by Rietveld refinement which was done with the program TOPAS 4.0.[3] The results of the refinement are presented in Figure S2 and Tables 1-3. Further data may be obtained from Fachinformationszentrum Karlsruhe, D-76344 Eggenstein-Leopoldshafen, Germany (fax: (+49)7247-808-666; e-mail: crysdata@fiz-karlsruhe.de) on quoting the depository numbers CSD-425643 ($LiBSi_2$).

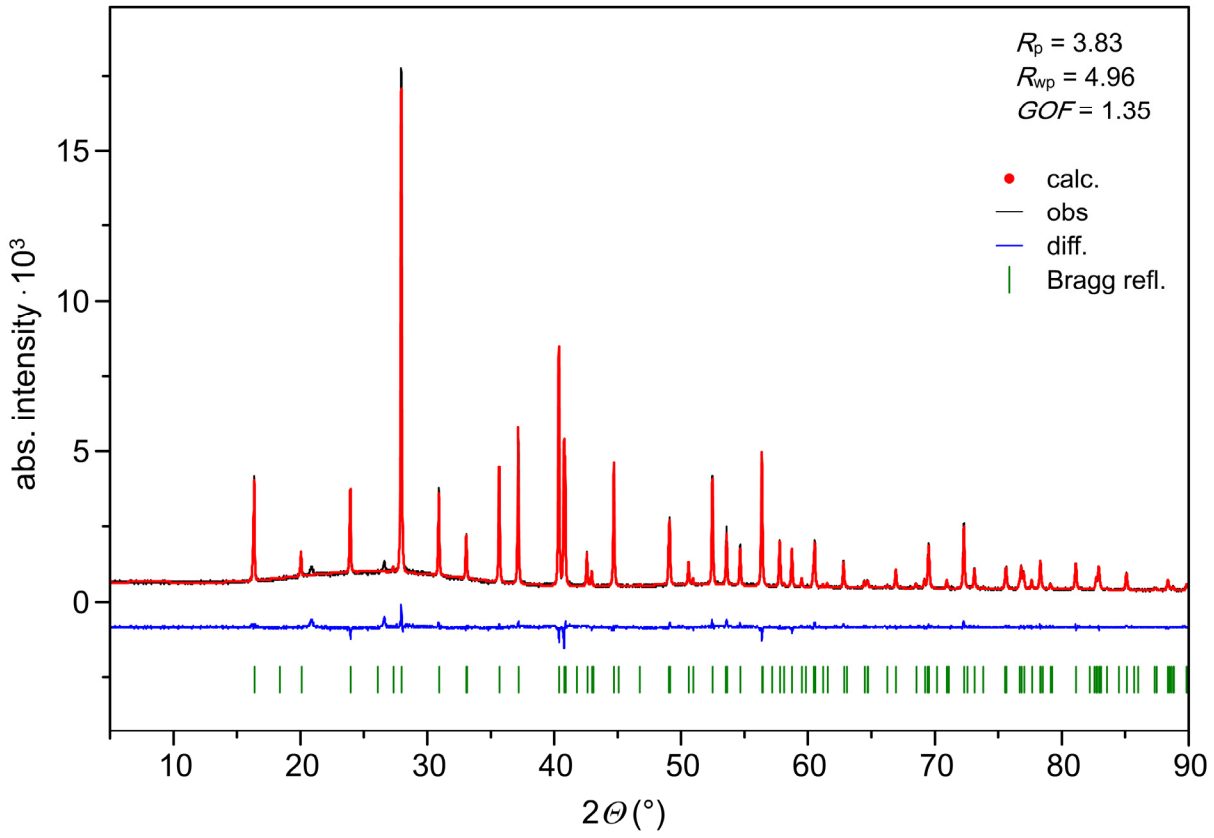

Figure S2. Experimental X-ray powder diffraction pattern of $LiBSi_2$ (black) referenced with the theoretical powder pattern based on Rietveld refinement (red). The difference plot is shown in blue.

Table 1. Crystallographic data of $LiBSi_2$ from Rietveld refinement ($P4_2/nmc$, $Z = 8$, origin at –1 (choice 2); estimated standard deviations in parentheses)

empirical formula	$LiBSi_2$
formula weight ($g \cdot mol^{-1}$)	73.92
space group	$P4_2/nmc$
unit cell dimension	a = 6.83225(3) Å, c = 8.83924(6) Å, V = 412.612(5) Å^3
Z	8
ρ (calc.) (g/cm^3)	2.38
μ (mm^{-1})	11.60
R_p / R_{wp} / GOF	3.83 / 4.96 / 1.35

Table 2. Fractional atomic coordinates, isotropic equivalent atomic displacement parameters and side occupancy factors for $LiBSi_2$ ($P4_2/nmc$, $Z = 8$, origin at –1 (choice 2); estimated standard deviations in parentheses).

Atom	Wyckoff position	*x*	*y*	*z*	*s.o.f.*	U_{iso} ($Å^2 \cdot 10^3$)
Li	8*g*	1/4	0.5042(9)	0.0784(5)	1	12(2)
B	8*f*	0.5095(3)	0.4905(3)	1/4	1	6(1)
Si1	8*g*	1/4	0.0690(1)	0.3632(1)	1	5.4(4)
Si2	8*g*	1/4	0.5665(1)	0.6181(1)	1	5.8(4)

Table 3. Interatomic distances in $LiBSi_2$ ($P4_2/nmc$, $Z = 8$, origin at –1 (choice 2); estimated standard deviations in parentheses).

Atom pair			*d*(Å)	Atom pair			*d*(Å)
Li-	B	2x	2.335(3)	Si1-	B1	2x	2.076(2)
	Si1		2.567(4)		Si2		2.436(1)
	Si2	2x	2.722(5)		Si1		2.474(1)
	Si2	2x	2.796(4)		Li		2.567(4)
	Si1	2x	2.799(4)		Li	2x	2.799(5)
	Si1	2x	2.857(5)		Li	2x	2.857(4)
B-	Si2	2x	2.052(2)	Si2-	B	2x	2.052(2)
	Si1	2x	2.076(2)		Si1		2.436(1)
	Li1	2x	2.335(5)		Si2		2.507(1)
					Li	2x	2.722(4)
					Li	2x	2.796(5)

Raman spectroscopy. Raman spectra were collected using a LabRAM HR 800 spectrometer. The instrument is equipped with an 800 mm focal length spectrograph and an air cooled (–70°C), back thinned CCD detector (pixel size 26x26 microns). The fine powdered sample was placed on a glass slide and the laser was focused onto the sample using a 50X super long working distance (WD=20.5 mm) Mitutoyo objective with a numerical aperture of 0.42 and depth of focus of 1.6 mm. The sample was excited using an air cooled double frequency Nd:YAG laser (532 nm, 5.6 mW) and an air cooled intra cavity regulated laser diode with point source (785 nm, 0.88 mW). The spectrum was collected with an exposure time of 60 sec, accumulation number of 10 and grating of 600 lines/mm.

Differential Scanning Calorimetry. Differential scanning calorimetry (DSC) measurements were performed with a NETZSCH DSC 404 Pegasus apparatus under an Ar gas flow of ~60 ml/min. About 5 mg of powder sample $LiBSi_2$ were sealed in a niobium crucible by arc-welding in an Ar-filled glove box. An empty niobium crucible served as reference. The scanning range was from room temperature to 800 °C with a heating/cooling rate of 10 K/min. The sample was recovered after the measurement and investigated by PXRD. Handling of DSC data was done with the program Proteus Thermal Analysis.[4] From the DSC trace and PXRD pattern of the recovered sample it could be concluded that $LiBSi_2$ does not decompose in the investigated temperature range.

Solid State Nuclear Magnetic Resonance (NMR) Spectroscopy. The ^{7}Li- and ^{11}B-MAS (magic angle spinning) NMR spectra (Figure S3 and S4) were collected on a Varian VNMRs 500 spectrometer operating at 160.37 MHz and 194.24 MHz for ^{11}B and ^{7}Li, respectively. MAS was performed at spinning speeds of 15 - 40 kHz employing a Varian 1.6 mm triple resonance T^{3}-MAS probe. $LiBSi_2$ appears as the only crystalline product beside an amorphous byproduct.

The ^{7}Li MAS NMR spectrum exhibits a signal at 0.95 ppm, accompanied by a set of spinning sidebands. From the positions of the outermost spinning sidebands a quadrupolar coupling constant C_Q = 0.18 MHz is estimated. At longer relaxation delays (up to 2h), a second contribution at -0.35 ppm adds to the signal.

In the ^{11}B-MAS NMR spectrum, a broad NMR signal appears centered around -0.5 ppm, with spinning sidebands covering a range of ± 0.8 MHz. In addition to this, a second contribution is found at -30.8 ppm, which exhibits a rather long relaxation time and but a small number of spinning sidebands. The quadrupolar coupling constants for these two components are estimated to C_Q= 1.6 MHz for the signal at -0.5 ppm and C_Q = 0.3 MHz for the narrow signal at -30.8 ppm. We tentatively assign the two signals with the long relaxation times (^{7}Li: -0.35 ppm; ^{11}B: -30.8 ppm) to $LiBSi_2$.

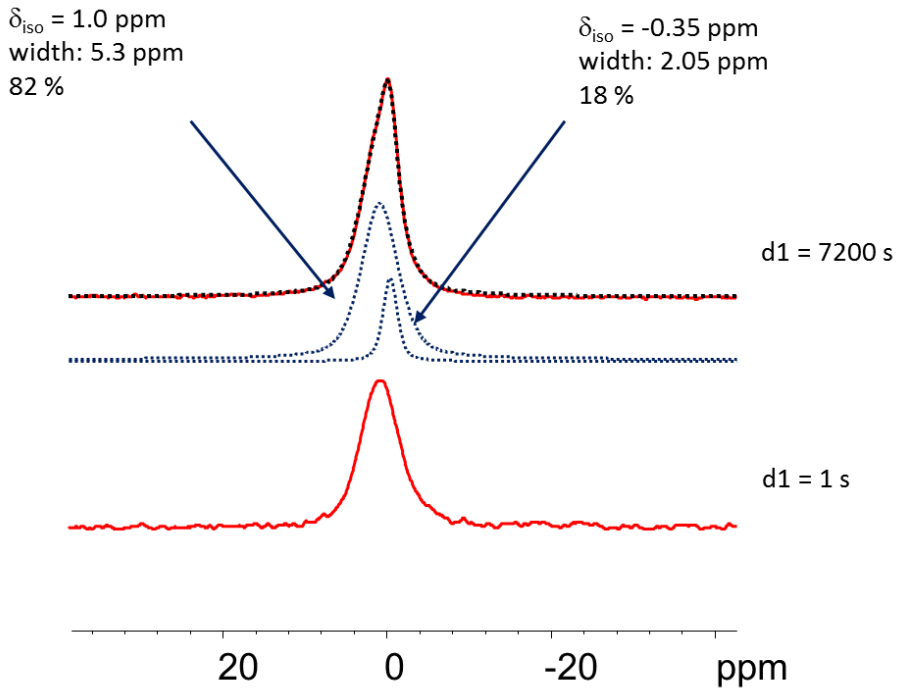

Figure S3: ^{7}Li-MAS NMR spectrum of $LiBSi_2$. Exp. details: ν_{RF} = 113.6 kHz; ν_{MAS} = 15 kHz; relaxation delay: 3600 s.

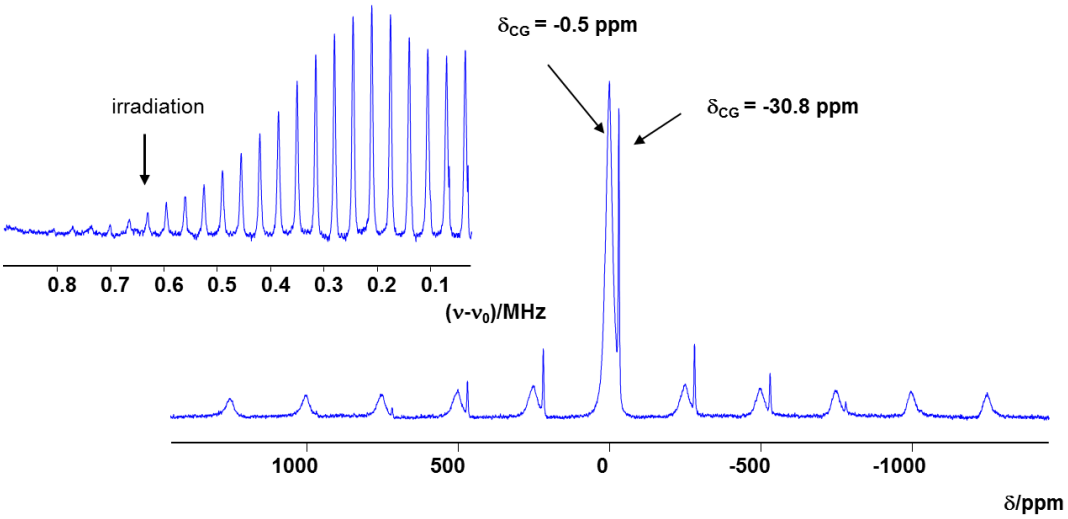

Figure S4: ^{11}B MAS NMR spectrum of $LiBSi_2$. Exp. details: ν_{RF} = 68.5 kHz; ν_{MAS} = 35 kHz; relaxation delay: 8000 s. Insert: sideband pattern for the broad component, from which a quadrupolar coupling constant C_Q = 1.6 MHz can be estimated (for I = 3/2, C_Q is identical to the overall width of the spectrum).

Computational details. Theoretical calculations of the electronic structure were performed using the first principles all-electron projected augmented wave (PAW) method[5] as implemented by the Vienna Ab Initio Simulation Package (VASP[6]). Exchange-correlation effects were treated within the generalized gradient approximation (GGA[7]) using the Perdew-Burke-Ernzerhof (PBE[8]) parameterization. The $LiBSi_2$ structure was relaxed with respect to volume, lattice parameters, and atom positions and using experimental parameters as starting values. Forces were converged to better than 1×10^{-3} eV/Å. The equilibrium volume was obtained by fitting to a third order Birch-Murnaghan equation of state.[9] The integration over the Brillion Zone (BZ) was done on a grid of special k-points with size 11×11×11 (6×6×6 for the equation of state) determined according to the Monkhorst-Pack scheme[10] and using the tetrahedron method with Blöchl correction.[11] The energy cutoff was set to 500 eV. Zone-centered phonon calculations were performed using VASP's density functional perturbation theory (DFPT) approach. The decomposition of the density of state (DOS) into atomic contributions is based on spheres with radii Li = 1.5 Å, Si = 1.25 Å, B = 0.8 Å, exceeding slightly the covalent radii of B and Si, and the ionic radius of Li (extrapolated to a coordination number 11). The structure parameters after relaxation and equations of states (EOS) parameters are specified in Tables S4 and S5. Note that the agreement with the experimental structure parameters is excellent (cf. Tables 1 and 2).

Table S4. Computationally relaxed structure parameters for $LiBSi_2$. Space group $P4_2/nmc$, a = 6.8328 Å, c = 8.8524 Å

Atom	Wyckoff position	*x*	*y*	*z*
Li	8*g*	1/4	0.5037	0.0766
B	8*f*	0.5080	0.4920	1/4
Si1	8*g*	1/4	0.0691	0.3637
Si2	8*g*	1/4	0.5663	0.6206

Table S5. Computed equation of states parameters:

	E_0 (eV/fu)	V_0 (Å^3/fu)	B_0 (GPa)	B_0'
Li_2BSi_2	-20.0308	51.702	103.7	4.1

References for Supporting Information

[1] E. Stoyanov, U. Häussermann, K. Leinenweber, *High Pressure Res.* **2010**, *30*, 175.
[2] a) F.O.X., Free Objects for Crystallography V 1.9.7.0, http://objcryst.sourceforge.net, **2011**; b) R. Cerny, V. Favre-Nicolin, *Powder Diffr.* **2005**, *20*, 359; c) V. Favre-Nicolin, R. Cerny, *J. Appl. Crystallogr.* **2002**, *35*, 734.
[3] TOPAS 4.0 - Rietveld Software, Bruker AXS, Madison (Wisconsin, USA), **2009**.
[4] Netzsch, Proteus Thermal Analysis V4.8.2, Netzsch-Gerätebau GmbH, Selb, Germany, **2006**.
[5] a) P. E. Blöchl, *Phys. Rev. B* **1994**, *50*, 17953; b) G. Kresse, D. Joubert, *Phys. Rev. B* **1999**, *59*, 1758.
[6] a) G. Kresse, J. Hafner, *Phys. Rev. B* **1993**, *48*, 13115; b) G. Kresse, J. Furthmüller, *Comp. Mater. Sci.* **1996**, *6*, 15.
[7] a) Y. Wang, J. P. Perdew, *Phys. Rev. B* **1991**, *44*, 13298; b) J. P. Perdew, J. A. Chevary, S. H. Vosko, K. A. Jackson, M. R. Pederson, D. J. Singh, C. Fiolhais, *Phys. Rev. B* **1992**, *46*, 6671.
[8] J. P. Perdew, K. Burke, M. Ernzerhof, *Phys. Rev. Lett.* **1996**, *77*, 3865.
[9] F. Birch, *Phys. Rev.* **1947**, *71*, 809.
[10] H. J. Monkhorst, J. D. Pack, *Phys. Rev. B* **1976**, *13*, 5188.
[11] P. E. Blöchl, O. Jepsen, O. K. Andersen, *Phys. Rev. B* **1994**, *49*, 16223.